

REDTEST: Towards Measuring Redundancy in Deep Neural Networks Effectively

Yao Lu^{1*} Peixin Zhang² Jingyi Wang³ Lei Ma^{4,5} Xiaoniu Yang¹ Qi Xuan^{1†}

¹Zhejiang University of Technology ²Singapore Management University

³Zhejiang University ⁴The University of Tokyo ⁵University of Alberta

Abstract

Deep learning has revolutionized computing in many real-world applications, arguably due to its remarkable performance and extreme convenience as an end-to-end solution. However, deep learning models can be costly to train and to use, especially for those large-scale models, making it necessary to optimize the original overly complicated models into smaller ones in scenarios with limited resources such as mobile applications or simply for resource saving. The key question in such model optimization is, how can we effectively identify and measure the redundancy in a deep learning model structure. While several common metrics exist in the popular model optimization techniques to measure the performance of models after optimization, they are not able to quantitatively inform the degree of remaining redundancy. To address the problem, we present a novel testing approach, i.e., REDTEST (short for Redundancy Testing), which proposes a novel testing metric called Model Structural Redundancy Score (MSRS) to quantitatively measure the degree of redundancy in a deep learning model structure. We first show that MSRS is effective in both revealing and assessing the redundancy issues in many state-of-the-art models, which urgently calls for model optimization. Then, we utilize MSRS to assist deep learning model developers in two practical application scenarios: 1) in Neural Architecture Search, we design a novel redundancy-aware algorithm to guide the search for the optimal model structure (regarding a given task) and demonstrate its effectiveness by comparing it to existing standard NAS practice; 2) in the pruning of large-scale pre-trained models, we prune the redundant layers of pre-trained models with the guidance of layer similarity to derive less redundant ones of much smaller size. Extensive experimental results demonstrate that removing such redundancy has a negligible effect on the model utility.

1. Introduction

Deep neural networks (DNNs) have achieved great success in many application scenarios including image understanding [19], object detection [40] and autonomous vehicle [32]. However, such success comes at a price, as the complex training process and the power consumption, especially those large-scale state-of-the-art models, can be costly, which requires significant computational and storage expense [8, 10]. For instance, on our experimental server, the storage space for ResNet152 with 60.2M parameters takes as much as 230.43 MB, and it would further take 226.06 MB memory and 11.56B Float Points Operations to infer the category of an image for the model. Such huge computation and storage consumption severely limits their deployment, especially on resource-constrained applications, e.g., mobile devices, or simply energy-critical scenarios.

To reduce the cost of deep learning applications, an intuitive way is to reduce the model size. In the ideal case, the model structure should be as simple as possible, to satisfy the utility requirement. Up to the present, we identify that existing research in machine learning community mostly follows the the following two main lines to achieve such a goal: *Model Pruning* (MP) and *Neural Architecture Search* (NAS). MP tries to remove the redundant part in the model structure, at different levels including weights [5, 13, 16, 29, 54], filters [14, 21, 26, 44, 47, 49] and layers [3, 21, 30, 31, 46, 49], based on their contributions to model inference. NAS adopts different search strategies, e.g., reinforcement learning [2, 36, 55, 58], evolutionary algorithm [28, 38, 39, 52] and gradient-based method [4, 25, 27], to guide the automatic selection of an optimal model structure, which balances between model accuracy and model size, from a large number of candidate models. Arguably, either for MP or NAS, the key challenge in reducing the model size is to effectively identify the redundant parts in the model structure. While existing MP and NAS techniques often leverage a set of metrics, e.g., the number of model parameters (Params) [3, 45], the re-

*yaolu.zjut@gmail.com

†Corresponding author: xuanqi@zjut.edu.cn, wangjiye@zju.edu.cn.

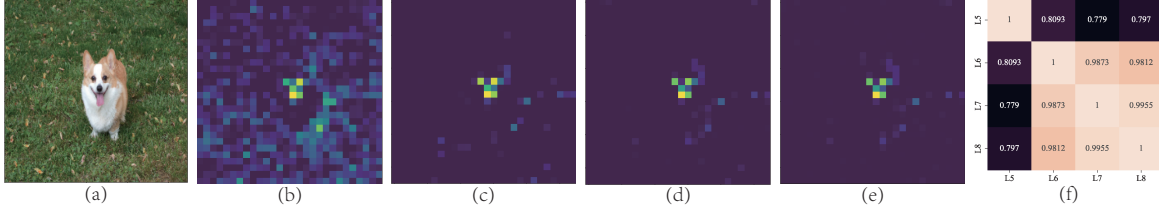


Figure 1. (a): Input image (224×224). (b)-(e): Visualization of IRs (28×28) in layers 5 to 8. (f): Similarity matrix. L_i denotes i -th layer.

quired Float Points Operations (FLOPs) [3, 26] and the time model takes to process one image (Latency) [45, 51], etc., to characterize the effectiveness of such model optimization, these existing metrics unfortunately can only measure the model complexity from different perspectives [20], but are not able to quantitatively measure the remaining redundancy. In other words, *they cannot characterize how far we are in obtaining a model with minimum redundancy.*

Unfortunately, so far, there still lacks a common consensus on the definition of redundancy, not to mention how to measure it effectively. To bridge this gap, in this paper, we first propose to leverage the similarity of intermediate representations (IRs) to reflect and characterize the structural redundancy of deep learning models. The motivation comes from an empirical and quantitative observation. As shown in Fig. 1, IRs learned by layer 6 to layer 8 of ResNet50 [19] are similar (either visually or quantitatively), indicating that these layers might be redundant in extracting useful information. Furthermore, we propose a novel testing metric to quantify the structural redundancy degree of DNNs, named *model structural redundancy score* (MSRS). MSRS can be used to calculate the similarity of any pair of IRs, even for those with different shapes (which can not be processed to calculate classical similarity metrics, e.g., cosine similarity and L_p -norm distance). Compared to existing metrics (e.g., Params, FLOPs and Latency used in model compression), MSRS is specially designed to assess and facilitate the identification of structural redundancy of models.

Equipped with MSRS, we finally present a novel testing framework, i.e., REDTEST, and apply REDTEST in two practical application scenarios to assist deep learning developers in developing better models: searching for the optimal model from scratch with NAS and pruning redundant large-scale pre-trained models. Our extensive experimental results demonstrate that REDTEST is helpful in identifying a better model by removing redundancy.

To summarize, we make the following contributions:

- We propose a novel testing metric called Model Structural Redundancy Score (MSRS) for deep learning models, which provides a quantitative assessment of the degree of redundancy in the model structure. With MSRS, we systematically explore and investigate the redundancy issue in state-of-the-art deep learning models and confirm

the ubiquitous presence of model redundancy, sometimes even to a surprisingly high level, which urgently calls for model structure optimization.

- We propose REDTEST, a *Redundancy Testing* framework, which provides an end-to-end solution for optimizing the model structure. Specifically, we consider two practical application scenarios: designing a model from scratch and shrinking a redundant pre-trained model. Specifically, we propose a redundancy-aware NAS algorithm on the basis of MSRS to search for better models with less structural redundancy. For the pruning of large-scale models, we design a new layer pruning method with the guidance of layer similarity to remove the structural redundancy.
- We release REDTEST together with all the experimental data publicly available¹, to benchmark and provide the basis for future study in this direction, which we believe to be important to contribute to a more energy-friendly deep learning ecosystem.

2. Preliminary

In this work, we consider two practical application scenarios for model optimization: MP and NAS. They share the same goal, i.e., balancing model accuracy and efficiency. However, they work in different scenarios: MP tries to shrink the model from a pre-trained one, leveraging both the architecture and parameters of the pre-trained model as prior knowledge, while NAS tries to search for a good model from scratch.

MP can be further categorized into weight pruning [13, 16, 29, 54], filter pruning [14, 21, 26, 44, 47, 49], and layer pruning [3, 21, 30, 49]. Weight pruning drops redundant weights to obtain sparse weight matrices, which has limited applications on general-purpose hardware [17]. Filter pruning seeks to remove unimportant filters according to specific metrics. However, FLOPs, Params, and Latency reduction by filter pruning are constrained by the original model’s depth. Hence, in this work, we focus on layer pruning, which eliminates entire redundant layers for better inference speedup.

NAS aims to search for the optimal architecture α for a

¹<https://anonymous.4open.science/r/RedTest-0318/>

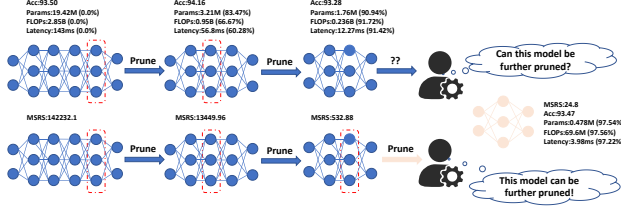


Figure 2. An intuitive example to explain the inadequacies of existing metrics.

given resource budget (e.g., latency) that achieves a desirable performance on the validation set among all candidate architectures S , which can be formulated as a bi-level optimization problem:

$$\begin{aligned} \min_{\alpha \in S} \mathcal{L}(\alpha, \theta_{\alpha}^*, \mathcal{D}_{val}) \\ \text{s.t. } \theta_{\alpha}^* = \min_{\theta_{\alpha}} \mathcal{L}(\alpha, \theta_{\alpha}, \mathcal{D}_{train}), \end{aligned} \quad (1)$$

where \mathcal{L} , θ_{α} , \mathcal{D}_{train} and \mathcal{D}_{val} denote the loss function (e.g., cross-entropy loss), the parameters of α , the training set and the validation set, respectively. Once α is found, it will be re-trained on \mathcal{D}_{train} (or $\mathcal{D}_{train} + \mathcal{D}_{val}$) and tested on the test set \mathcal{D}_{test} .

3. Motivation and Research Objective

In this section, we present the motivation of REDTEST along with its two practical application scenarios.

3.1. Motivation

The motivation for designing MSRS stems from the observation that existing metrics in measuring model optimization, e.g., Params, FLOPs and Latency can only quantify the model complexity (after optimization), but are unable to quantitatively measure the structural redundancy in deep learning models. For ease of understanding, we take Fig. 2 as an example to intuitively illustrate the limitation of existing metrics in practice. We observe that the model complexity decreases and the model accuracy still maintains at an acceptable level as the model is gradually pruned. However, the developer can struggle to determine whether the model can be further optimized without a measurement of the redundancy of the current model. For example, in the extreme case of our experiments, even if the model complexity is reduced to 10% of the original (i.e., 90.94% parameters reduction, 91.72% FLOPs reduction and 91.42% Latency reduction), the model still yields 93.28% top-1 accuracy, i.e., only with a slight accuracy drop. Our proposed redundancy measurement metric MSRS complements existing performance metrics and enables a developer to be aware of the model optimization progress.

3.2. Application Scenarios.

Nowadays, there are numerous well-designed models offered by PyTorch [35], TensorFlow [1] and third-party libraries [9, 50], or pre-trained models from open-source resources, e.g., OpenVINO². However, many of these models are overly complicated and can not be directly deployed on resource-constrained devices such as mobile or embedded devices due to the high computational cost.

REDTEST is designed to work in any real-world setting where deep learning developers want a more lightweight model for suiting a specific task. It is worth noting that REDTEST is regarded as a static analysis tool where both the computational graph and the model parameters are fixed once trained. Here, we provide the following two potential scenarios with numerical applications:

- **Application Scenario 1 (AS1):** Deep learning developers want to design suitable models from scratch to meet both the accuracy and computational requirement.
- **Application Scenario 2 (AS2):** Deep learning developers want to prune large-scale pre-trained models without sacrificing too much accuracy to reduce as much resource consumption as possible.

4. The Proposed REDTEST

The core of our proposed REDTEST is a testing metric called MSRS to quantitatively measure model structural redundancy. Utilizing MSRS, we further provide two typical application scenarios: 1) searching for the optimal model from scratch, and 2) optimizing redundant pre-trained models.

4.1. The MSRS Measurement

The key idea of MSRS is to measure the similarities of IRs. The intuition is that the IRs store interesting information for the learning task and their mutual similarities can be useful to measure the redundancy in the model structure from an information extraction perspective. The higher the similarity is, the larger redundancy of the model structure is.

Note that since the output shapes of different hidden layers are various, it is impractical to utilize traditional metrics, such as cosine similarity and euclidean distance to directly measure the similarity between two IRs. We adopt Centered Kernel Alignment (CKA) [23] to address this challenge. Given two IRs, $F_i \in \mathbb{R}^{n \times p_i}$ and $F_j \in \mathbb{R}^{n \times p_j}$, one with p_i neurons in i -th layer and another p_j neurons in j -th layer, to the same n samples, we measure the similarity between each pair of inputs through gram matrices $S_i = F_i F_i^T$ and $S_j = F_j F_j^T$. It is worth noting that the order of the gram matrix $S \in \mathbb{R}^{n \times n}$ is only related to n , i.e., it can avoid the problem of misalignment caused by different output shapes

²https://github.com/openvinotoolkit/open_model_zoo

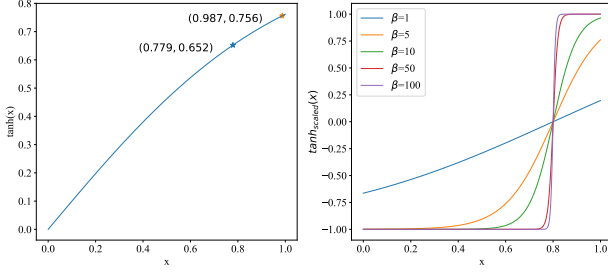


Figure 3. Representations of hyperbolic tangent function in $[0, 1]$ and scaled hyperbolic tangent functions for $\epsilon = 0.8$ and various choices of β .

of hidden layers. Next, we adopt Hilbert-Schmidt Independence Criterion (HSIC) [15] to calculate the statistical independence of S_i and S_j .

$$HSIC_0(S_i, S_j) = \frac{1}{(n-1)^2} \text{tr}(S_i H S_j H), \quad (2)$$

where $H = I_n - \frac{1}{n} \mathbf{1}\mathbf{1}^T$ is the centering matrix. We refer readers to [15] for detailed derivation. However, $HSIC_0$ is not invariant to isotropic scaling, which is the basic requirement of similarity metric [23]. Thus, we further normalize $HSIC_0$ using Eq. (3):

$$CKA_0(S_i, S_j) = \frac{HSIC_0(S_i, S_j)}{\sqrt{HSIC_0(S_i, S_i)} \sqrt{HSIC_0(S_j, S_j)}} \quad (3)$$

Another limitation of $HSIC_0(S_i, S_j)$ is that it has $O(\frac{1}{n})$ bias [15], where n denotes the number of samples. In order to make the value independent of the batch size, we replace $HSIC_0(S_i, S_j)$ with an unbiased one [43], which is depicted as follows:

$$HSIC_1(S_i, S_j) = \frac{1}{n(n-3)} \left[\text{tr}(\tilde{S}_i \tilde{S}_j) + \frac{\mathbf{1}^T \tilde{S}_i \mathbf{1} \mathbf{1}^T \tilde{S}_j \mathbf{1}}{(n-1)(n-2)} - \frac{2}{n-2} \mathbf{1}^T \tilde{S}_i \tilde{S}_j \mathbf{1} \right], \quad (4)$$

where \tilde{S}_i and \tilde{S}_j are derived from setting the diagonal entries of S_i and S_j to zero. Finally, unbiased CKA can be computed as follows:

$$CKA_1(S_i, S_j) = \frac{HSIC_1(S_i, S_j)}{\sqrt{HSIC_1(S_i, S_i)} \sqrt{HSIC_1(S_j, S_j)}}, \quad (5)$$

whose value ranges from 0 to 1 and a higher value is preferred.

After obtaining the similarities between IRs, we further design a scoring mechanism to directly measure the redundancy degree. As shown in Fig. 1, high similarity values reveal that the corresponding layers expose high redundancy. Hence, we prioritize high similarity values and assign higher weights to them. One widely adopted way in

Algorithm 1: The MSRS Measurement

Input: IRs set $\{F_1, F_2, \dots, F_l\}$
Input: model-specific threshold ϵ
Input: scaling factor β

- 1 Initialize MSRS=0;
- 2 **for** $i = 1$ to l **do**
- 3 $S_i = F_i F_i^T$
- 4 **for** $j = 1$ to l **do**
- 5 $S_j = F_j F_j^T$
- 6 $x = \frac{HSIC_1(S_i, S_j)}{\sqrt{HSIC_1(S_i, S_i)} \sqrt{HSIC_1(S_j, S_j)}}$
- 7 **if** $i > j$ **then**
- 8 $score = \frac{\exp(\beta(x-\epsilon)) - \exp(-\beta(x-\epsilon))}{\exp(\beta(x-\epsilon)) + \exp(-\beta(x-\epsilon))}$
- 9 $score = 0.5 \times score + 0.5$
- 10 $MSRS += score$
- 11 **end**
- 12 **end**
- 13 **end**
- 14 **return** MSRS

deep learning research is to use hyperbolic tangent function [11, 22]. However, hyperbolic tangent function can not be directly applied here for two reasons: 1) The Eq. (5) value is in $[0, 1]$. If we use hyperbolic tangent function directly, those low similarity values have a non-negligible impact. For example, the assigned score (see the left plot of Fig. 3) is 0.652 for $x = 0.779$, 0.756 for $x = 0.987$. Although the numerical difference between 0.652 and 0.756 is small, their similarity degrees are fundamentally different (see Fig. 1). 2) It can be difficult to set a global similarity threshold to decide whether there are redundant layers because similarities between IRs may differ across various model structures in the real world.

To address the problem, we adapt the original hyperbolic tangent function by introducing two hyperparameters: a scaling factor β and a model-specific threshold ϵ .

$$\tanh_{scaled}(x) = \frac{\exp(\beta(x-\epsilon)) - \exp(-\beta(x-\epsilon))}{\exp(\beta(x-\epsilon)) + \exp(-\beta(x-\epsilon))} \quad (6)$$

Specifically, the scaling factor β controls the assigned score of the low similarity value. As β increases, the effect of low similarity values on redundancy gradually decreases (see the right plot of Fig. 3). When β tends to infinity, Eq. (6) is equivalent to $\text{sign}(x - \epsilon)$. As for model-specific threshold ϵ , we use various ϵ for different model structures. Empirical rules for picking β and ϵ are summarized in RQ4.

We provide a summary of calculating MSRS in Algorithm 1. Given a series of IRs $\{F_1, F_2, \dots, F_l\}$, model-specific threshold ϵ and scaling factor β , we first initialize MSRS to 0. Then, we traverse IRs set twice to calculate gram matrices for the corresponding IRs (see line 3 and 5).

Algorithm 2: Redundancy-aware NAS

Input: candidate architectures $\{m_1, m_2, \dots, m_n\}$
Input: expected MSRS M
Input: expected Latency T
Input: a tunable hyperparameter λ
Input: weight factor w

```

1 Initialize  $best\_model = \emptyset, best\_score = 0$ 
2 for  $i = 1$  to  $n$  do
3   Using Algorithm 1 to calculate the MSRS of  $m_i$ 
4    $score = ACC(m_i) \times$ 
      $\left[ \lambda \times \frac{LAT(m_i)}{T} + (1 - \lambda) \times \frac{MSRS(m_i)}{M} \right]^w$ 
5   if  $score > best\_score$  then
6      $best\_model = m_i$ 
7      $best\_score = score$ 
8   end
9 end
10 return  $best\_model$ 
```

Next, we utilize each pair of gram matrices, i.e. S_i and S_j , to calculate $CKA_{unbiased}$ (For simplicity, we use x denotes $CKA_{unbiased}$) at line 6. Once the condition that $i > j$ is satisfied, we feed x into the scaled hyperbolic tangent function to obtain a corresponding score (see line 8) and normalize it (see line 9). Finally, we sum up all obtained scores at line 10 to derive MSRS.

4.2. AS1: Redundancy-aware NAS

Designing redundancy-aware algorithms capable of automating the discovery of optimal architectures is critical for NAS to tradeoff between performance and the resource budget. Extensive prior research [45, 51, 53] has been explored in the direction of NAS to find a Pareto optimal solution by incorporating different metrics into the scoring function, e.g., Latency [45] as follows.

$$\max_m ACC(m) \times \left[\frac{LAT(m)}{T} \right]^w, \quad (7)$$

where $ACC(m)$, $LAT(m)$, T and w denote the accuracy of model m on the specified dataset, the Latency of model m on the specified device, expected Latency and application-specific constant, respectively. See [45] for the empirical rule of thumb for picking w . In Sec. 3.1, we have clarified the insufficiency of existing metrics including Params, FLOPs, and Latency. To design redundancy-aware NAS, we propose to incorporate MSRS into the scoring function based on Eq. (7).

$$\max_m ACC(m) \times \left[\lambda \times \frac{LAT(m)}{T} + (1 - \lambda) \times \frac{MSRS(m)}{M} \right]^w, \quad (8)$$

where $MSRS(m)$, M and λ denote MSRS of model m , expected MSRS and a tunable hyperparameter. However,

Algorithm 3: Redundancy-aware layer pruning

Input: IRs set $\{F_1, F_2, \dots, F_l\}$
Input: similarity threshold μ :

```

1 Initialize  $remained\_layer = \emptyset, cur = i = 1$ 
2 while  $i < l$  do
3    $i++$ 
4    $S_{cur} = F_{cur} F_{cur}^T$ 
5    $S_i = F_i F_i^T$ 
6    $CKA_{unbiased} =$ 
      $\frac{HSIC_1(S_{cur}, S_i)}{\sqrt{HSIC_1(S_{cur}, S_{cur})} \sqrt{HSIC_1(S_i, S_i)}}$ 
7   if  $CKA_{unbiased} < \mu$  then
8      $remained\_layer = remained\_layer \cup cur$ 
9   end
10   $cur = i$ 
11 end
12 return  $remained\_layer$ 
```

unlike expected Latency T can be set according to real scenarios, it is difficult to propose a budget for expected MSRS M . To resolve this issue, we provide an empirical guide to picking expected MSRS in Appendix B.

We integrate the designed score into the NAS algorithm (see in Algorithm 2). To be specific, we first initialize the best model and score as \emptyset and 0 in line 1. Then, we traverse all candidate architectures, apply Algorithm 1 to calculate MSRS for each candidate architecture, and score it using Eq. (8) (see line 3 and 4). If the current score is greater than the best score, we update the best model and score to the current model and score, respectively (see lines 5 - 8). Finally, we obtain the model with the highest score in line 10.

4.3. AS2: Redundancy-aware Layer Pruning

In Sec. 4.1, we obtain an MSRS for the target model, which reflects the structural redundancy in this model. For those highly redundant models, we design a brand new layer pruning method to optimize their model structures.

Different from existing layer pruning methods, our method builds upon the layer similarity between two adjacent layers. We prefer to retain the shallower layer of two adjacent layers to ensure the correctness of the prediction as much as possible. For ease of understanding, we provide an example as follows. Let F_{i-1} , F_i and F_{i+1} be the outputs of three consecutive layers L_{i-1} , L_i and L_{i+1} , respectively. We assume $F_i \sim F_{i+1}$, thus removing L_{i+1} has less impact on subsequent inference of the model. On the contrary, if we discard L_i , then F_{i-1} becomes the input of L_{i+1} and the corresponding output now is $f_{i+1}(F_{i-1})$ (f_{i+1} is the feature extraction function of $i+1$ -th layer), which is totally different from F_{i+1} , since F_{i-1} and F_i are not similar. Algorithm 3 presents the details of our layer pruning method. We first initialize the remaining and cur-

rent layers as \emptyset and 1, respectively. Next, we traverse IRs and calculate the layer similarity between the current layer and its next layer (see lines 4-6). If the unbiased CKA is smaller than the predefined similarity threshold μ , we keep the current layer in the resultant model, otherwise, discard it (see line 8). Afterwards, we update the current layer to its next layer in line 10 and continue the loop. Due to the layer drop, two consecutive layers in the resulting model may have dimensional mismatches. We thus modify the latter layer to match the front layer and finally obtain a model with as little redundancy as possible in line 12. As for the compact model, we randomly initialize the parameters of those layers that changed dimensions and reuse the weights of pre-trained models for other layers.

5. Experimental Evaluation

We conduct experiments on four popular and publicly-available datasets including CIFAR10 [24], CIFAR100 [24], ImageNet [41] and ImageNet16-120 [6]. If not specified, we set the initial learning rate, batch size, weight decay, epoch and momentum to 0.01, 256, 0.005, 150 and 0.9, respectively. The learning rate is decayed by a factor of 0.1 at epochs 50 and 100. Besides, we utilize stochastic gradient descent algorithm to optimize the model. In total, we systematically measure the model structural redundancy over 35,000 DNN models to demonstrate the effectiveness of MSRS.

How effective is MSRS in measuring structural redundancy? To answer the question, we compare MSRS with existing metrics, e.g., FLOPs, Params and Latency, in measuring a family of models whose redundancy increases gradually. Specifically, we conduct experiments on the CIFAR10 and CIFAR100 dataset with a family of ResNets of different layers. Intuitively, as the number of layers increases, the ResNet model is transiting from underfitting to overfitting for the given learning task and the model redundancy is expected to grow at some point in the middle (where a model structure fits the task well). As shown in Fig. 4a, ResNet5, ResNet8 and ResNet10 are still underfitting as indicated by their test accuracy, which have little redundancy. This matches their MSRS score well (all below 1 (see Fig. 4c)). Furthermore, as the model complexity grows from ResNet10 to ResNet56, the model redundancy does grow significantly from a certain point in the middle as we expected. For instance, when the model has over 1,000 layers, it tends to be overfitting and overparameterized (93.78% of ResNet110 vs. 91.46% of ResNet1202). Meanwhile, the MSRS of ResNet1202 becomes extremely high, i.e., 95,817. These observations confirm that our designed MSRS is strongly correlated with the model structural redundancy. In contrast, FLOPs, Params and Latency are simply proportional to the model depth (see Fig. 4b), which is ineffective in revealing the structural redundancy

issues. We can draw the same conclusion on CIFAR100 (See Fig. E6 in Appendix for space reasons).

We further explore the structural redundancy in widely used ResNets [19] and VGGs [42] models for image classification. For the ImageNet dataset, we utilize pre-trained models from torchvision³ to calculate MSRS. For CIFAR10 and CIFAR100, we train models from scratch. The performance of the above models is summarized in Tab. E6 of Appendix. To unify the coordinate axis scale, we take the binary logarithm of the calculated MSRS. The results are shown in Fig. 5. We could observe that as the model (for both ResNets and VGGs) goes deeper, the degree of structural redundancy increases accordingly for CIFAR10, CIFAR100 and ImageNet. A closer look reveals that although many models achieve comparable performance, their MSRSs vary significantly. MSRS provides a new dimension to evaluate and further optimize the model quality. For instance, the model accuracy of ResNet56 and ResNet110 on CIFAR10 are almost the same (93.11% vs. 93.78%), while their MSRSs are quite different (140.77 vs. 708.12). The underlying reason is that there are certain layers in ResNet110 extracting similar features leading to structural redundancy in the model.

Summary: MSRS is effective in measuring and revealing model structural redundancy, which is present (sometimes to a surprisingly high level) in many popular models.

How useful is MSRS in assisting NAS for the search of models with appropriate structure? To answer this question, we conduct experiments on NATS-Bench [9], a relatively fair and unified benchmark for the comparison of different NAS algorithms. With the provision of extra statistics, such as accuracy during training and Latency, running NAS algorithms on NATS-Bench can avoid the expensive computational overhead of training the architecture via directly querying from the database. Herein, we compare our redundancy-aware NAS algorithm (S3) with another two algorithms to evaluate its validity: S1 [27, 39, 57] focuses on achieving higher accuracy, regardless of the associated resource budget, e.g., FLOPs, Params and Latency. S2 [45] investigates a resource-aware NAS algorithm to tradeoff accuracy against resource consumption (Latency).

Specifically, we respectively sample as many as 11,715, 11,748 and 11,741 valid architecture candidates on CIFAR10, CIFAR100 and ImageNet16-120 on NATS-Bench with a topology search space and utilize Algorithm 2 to select 1% top-ranking models (See Tab. E2 for detailed parameter settings). To be fair, we use the same w and T for S2 and our redundancy-aware NAS algorithm. Since final

³<https://pytorch.org/vision/stable/index.html>

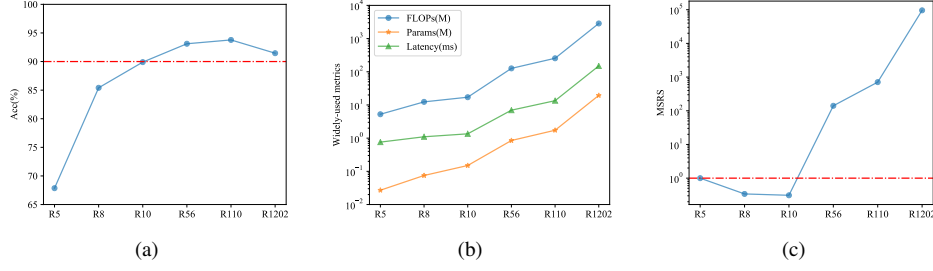


Figure 4. Differences between existing metrics and MSRS for a family of ResNets on CIFAR10. R denotes ResNet.

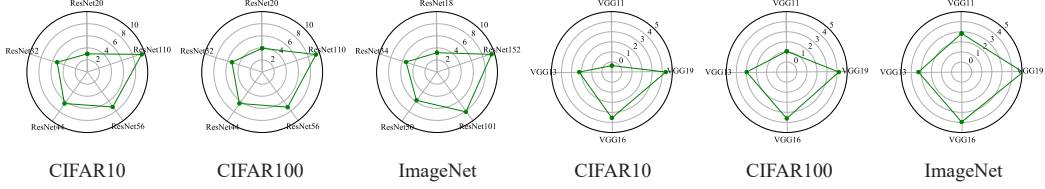


Figure 5. Structural redundancy in widely-used backbones on various datasets. To unify the coordinate axis scale, we take the binary logarithm of the calculated MSRS.

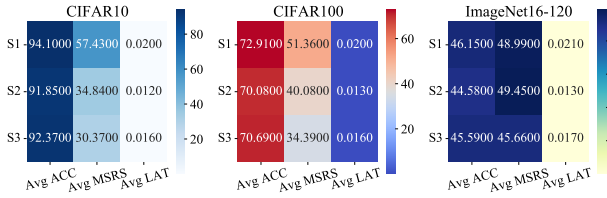


Figure 6. Statistics of top-ranking models in NATS-Bench selected by different strategies. Avg ACC (%), Avg MSRS and Avg LAT (s) represent average accuracy, average MSRS and average Latency.

accuracy can be impractical to evaluate the relative ranking of such a large number of architectures, we use the accuracy of the 12-th epoch to approximate the final accuracy of each candidate [9], which allows us to perform architecture search quickly.

Then, we calculate the average value of accuracy, MSRS and Latency of top-ranking models selected by various NAS algorithms (see Fig. 6). According to the experimental results, we observe that models selected by S1 have the highest average value on accuracy (94.10% on CIFAR10, 72.91% on CIFAR100 and 46.15% on ImageNet16-120), Latency (0.02 on CIFAR10, CIFAR100 and 0.021 on ImageNet16-120) and MSRS (57.43 on CIFAR10, 51.36 on CIFAR100 and 48.99 on ImageNet16-120), which is attributed to the fact that S1 only focuses on accuracy but ignores the accompanying resource overhead. By contrast, S2 seeks to find the Pareto-optimal solutions to achieve accuracy-Latency trade-offs. Hence, the models selected by S2 can achieve lower Latency but exhibit an accuracy drop compared to S1. Specifically, the average accuracies and Latencies obtained by S2 are 91.85% and 0.012 on CIFAR10, 70.08% and 0.013 on CIFAR100 as well as 44.58%

and 0.013 on ImageNet16-120. Besides, we observe that S2 can eliminate model structural redundancy to a certain extent. However, since Latency cannot accurately reflect the structural redundancy existing in the models, models selected by S2 exhibit higher MSRS than S3 (our redundancy-aware NAS algorithm). Specifically, in comparison with S2, models selected by S3 have less structural redundancy (30.37 vs. 34.84 on CIFAR10, 34.39 vs. 40.08 on CIFAR100 and 45.66 vs. 49.45 on ImageNet16-120) while yielding higher accuracy (92.37% vs. 91.85% on CIFAR10, 70.69% vs. 70.08% on CIFAR100 and 45.59% vs. 44.58% on ImageNet16-120). Note that, the effectiveness of MSRS-assisted NAS in finding better models (with overall 30000 models evaluated) further confirms the usefulness of MSRS in measuring the redundancy. In Appendix A, we further incorporate Params and FLOPs into the scoring function to evaluate the effectiveness of the redundancy-aware NAS algorithm.

Summary: Compared to existing standard practice, our redundancy-aware NAS algorithm with the assistance of MSRS is able to find better models with less redundancy while sacrificing as little accuracy as possible.

How effective is redundancy-aware layer pruning in reducing the model’s structural redundancy? We answer this question from two aspects. First, we conduct experiments on pruning with the guidance of layer similarity to evaluate the effectiveness of our redundancy-aware layer pruning in alleviating the model structural redun-

dancy. Specifically, we utilize Algorithm 3 to obtain models with little redundancy and then fine-tune them. All the hyperparameter settings are the same as normal training. For each model, we run three times and report the mean and standard deviation to avoid the effect of randomness. As an example, we visualize the results of CKA diagnosis on CIFAR10 with VGG19 and ResNet56 in Fig. E3 of Appendix. Layers with high CKA values are labeled with a transparent color and are considered redundant. To evaluate the effectiveness of our method, we compare the performance with existing state-of-the-art layer pruning methods [3, 30, 48] in terms of accuracy and FLOPs/Params/Latency reduction. We re-implemented these baselines following the guidance and configurations of the original papers. We use these methods to select non-redundant layers on the same model and fine-tune the resulting model with the same setting as ours. For a fair comparison, we do not use the performance recovery strategies, such as knowledge distillation in [3, 48] and iterative pruning in [48].

Tab. 1 summarizes the experimental results of VGG19 and ResNet56 on CIFAR10. Generally, our redundancy-aware layer pruning surpasses the baselines. More specifically, as for ResNet56, 52.60% FLOPs, 45.00% parameters and 50.78% Latency are removed by us, while it still yields 93.40% top-1 accuracy. Compared with Chen et al.[3] and DBP[48], our method achieves better accuracy, FLOPs and Latency reduction, while maintaining the same parameters reduction. Note that the difference between Chen et al. and DBP lies in the techniques to recover the performance. Besides, although our method is slightly inferior to Lu et al. [30] in FLOPs and Latency reduction, our method maintains better parameters reduction and better accuracy. As for VGG19, our method surpasses Lu et al. in all aspects, including top-1 accuracy, as well as FLOPs, parameters and Latency reduction (93.01% vs. 91.7% for accuracy, 54.41% vs. 35.51% for FLOPs, 63.34% vs. 46.82% for parameters and 40.16% vs. 31.10% for Latency). Finally, in comparison with Chen et al. and DBP, our redundancy-aware layer pruning has better accuracy, FLOPs and Latency reduction, while Chen et al. and DBP show more advantages in reduction of parameters. Furthermore, our method also surpasses the baselines on CIFAR100 (See Tab. E5 in Appendix for space reasons). Hence, our method works well in alleviating the model structural redundancy. The above experiments in turn confirm that these high-similarity layers are redundant and can be pruned with minimal impact on model accuracy with the guidance of MSRS.

After demonstrating the effectiveness of our redundancy-aware layer pruning, we further investigate structural redundancy in pruned models. Hence, we calculate the MSRS for pruned models obtained by various layer pruning methods and measure the corresponding MSRS reduction compared with original models. The results are shown in Fig. E2,

Model	Method	Top-1%	Params (PR)	FLOPs (PR)	Latency (PR)
ResNet56	Original	93.11	0%	0%	0%
	Chen et al. [3]/DBP [48]	92.79 \pm 0.13	45.00%	41.30%	38.76%
	Lu et al. [30]	92.7 \pm 0.04	42.91%	60.23%	55.87%
	Ours	93.40 \pm 0.05	45.00%	52.60%	50.78%
VGG19	Original	93.36	0%	0%	0%
	Chen et al. [3]/DBP [48]	92.86 \pm 0.17	69.62%	44.92%	35.83%
	Lu et al. [30]	91.71 \pm 0.13	46.82%	35.51%	31.10%
	Ours	93.01 \pm 0.17	63.34%	54.41%	40.16%

Table 1. Comparison of different layer methods.

from which we find that the model structural redundancy is mitigated to varying degrees. Specifically, the original MSRS of ResNet56 and VGG19 on CIFAR10 are 140.77 and 20.39. Model structural redundancy completely disappears after applying layer pruning to ResNet56 (MSRS reduction is 100% for all methods). By contrast, although the effect of mitigating model structural redundancy on VGG19 is not as good as on ResNet56, it also fully demonstrates the capability of existing layer pruning methods in reducing the structural redundancy of deep learning models (The MSRS reductions of Chen et al. and DBP, Lu et al. and ours are 91.5%, 73.3% and 98.4%, respectively). Among these methods, our method achieves the best results, which further demonstrates the effectiveness of our redundancy-aware layer pruning.

Summary: Layer pruning is helpful for alleviating model structural redundancy to varying degrees, especially effective for models with high levels of redundancy. In addition, experiments demonstrate the effectiveness of our redundancy-aware layer pruning in reducing the model complexity.

6. Conclusion

In this work, we develop REDTEST, a novel *Redundancy Testing* framework, to measure the deep learning model’s structural redundancy and help model developers to optimize the model structure. We first show that MSRS is effective in both revealing and assessing the redundancy issues in many state-of-the-art backbones, which urgently call for model optimization. Then, we further propose model optimization techniques to help assist model developers in two practical application scenarios: 1) in NAS, we propose a redundancy-aware NAS algorithm to guide the search for the optimal structure and show its effectiveness by comparing it to existing standard NAS practice; 2) in MP, we design a redundancy-aware layer pruning with the guidance of MSRS to prune the redundant layers of pre-trained models. Extensive experiments demonstrate that removing such redundancy has a negligible effect on the model utility. We hope that REDTEST can facilitate a much larger community of researchers to concentrate on optimizing model structures in a more computationally effective environment and ultimately create a greener deep learning ecosystem.

References

- [1] Martín Abadi, Paul Barham, Jianmin Chen, Zhifeng Chen, Andy Davis, Jeffrey Dean, Matthieu Devin, Sanjay Ghemawat, Geoffrey Irving, Michael Isard, Manjunath Kudlur, Josh Levenberg, Rajat Monga, Sherry Moore, Derek Gordon Murray, Benoit Steiner, Paul A. Tucker, Vijay Vasudevan, Pete Warden, Martin Wicke, Yuan Yu, and Xiaoqiang Zheng. Tensorflow: A system for large-scale machine learning. In *12th USENIX Symposium on Operating Systems Design and Implementation, OSDI 2016, Savannah, GA, USA, November 2-4, 2016*, pages 265–283. USENIX Association, 2016. 3
- [2] Bowen Baker, Otkrist Gupta, Nikhil Naik, and Ramesh Raskar. Designing neural network architectures using reinforcement learning. In *5th International Conference on Learning Representations, ICLR 2017, Toulon, France, April 24-26, 2017, Conference Track Proceedings*. OpenReview.net, 2017. 1, 14
- [3] Shi Chen and Qi Zhao. Shallowing deep networks: Layer-wise pruning based on feature representations. *IEEE transactions on pattern analysis and machine intelligence*, 41(12): 3048–3056, 2018. 1, 2, 8, 13, 15
- [4] Xin Chen, Lingxi Xie, Jun Wu, and Qi Tian. Progressive differentiable architecture search: Bridging the depth gap between search and evaluation. In *2019 IEEE/CVF International Conference on Computer Vision, ICCV 2019, Seoul, Korea (South), October 27 - November 2, 2019*, pages 1294–1303. IEEE, 2019. 1, 14
- [5] Zhuangzhi Chen, Jingyang Xiang, Yao Lu, Qi Xuan, Zhen Wang, Guanrong Chen, and Xiaoniu Yang. Rgp: Neural network pruning through regular graph with edges swapping. *IEEE Transactions on Neural Networks and Learning Systems*, 2023. 1
- [6] Patryk Chrabaszcz, Ilya Loshchilov, and Frank Hutter. A downsampled variant of imagenet as an alternative to the cifar datasets. *arXiv preprint arXiv:1707.08819*, 2017. 6, 14
- [7] Josen Daniel De Leon and Rowel Atienza. Depth pruning with auxiliary networks for tinymml. In *ICASSP 2022-2022 IEEE International Conference on Acoustics, Speech and Signal Processing (ICASSP)*, pages 3963–3967. IEEE, 2022. 13
- [8] Jacob Devlin, Ming-Wei Chang, Kenton Lee, and Kristina Toutanova. BERT: pre-training of deep bidirectional transformers for language understanding. In *Proceedings of the 2019 Conference of the North American Chapter of the Association for Computational Linguistics: Human Language Technologies, NAACL-HLT 2019, Minneapolis, MN, USA, June 2-7, 2019, Volume 1*, pages 4171–4186. Association for Computational Linguistics, 2019. 1
- [9] Xuanyi Dong, Lu Liu, Katarzyna Musial, and Bogdan Gabrys. Nats-bench: Benchmarking nas algorithms for architecture topology and size. *IEEE transactions on pattern analysis and machine intelligence*, 2021. 3, 6, 7
- [10] Alexey Dosovitskiy, Lucas Beyer, Alexander Kolesnikov, Dirk Weissenborn, Xiaohua Zhai, Thomas Unterthiner, Mostafa Dehghani, Matthias Minderer, Georg Heigold, Sylvain Gelly, Jakob Uszkoreit, and Neil Houlsby. An image is worth 16x16 words: Transformers for image recognition at scale. In *9th International Conference on Learning Representations, ICLR 2021, Austria, May 3-7, 2021*. OpenReview.net, 2021. 1
- [11] Shiv Ram Dubey, Satish Kumar Singh, and Bidyut Baran Chaudhuri. A comprehensive survey and performance analysis of activation functions in deep learning. *arXiv preprint arXiv:2109.14545*, 2021. 4
- [12] Sara Elkerdawy, Mostafa Elhoushi, Abhineet Singh, Hong Zhang, and Nilanjan Ray. One-shot layer-wise accuracy approximation for layer pruning. In *2020 IEEE International Conference on Image Processing (ICIP)*, pages 2940–2944. IEEE, 2020. 13
- [13] Jonathan Frankle and Michael Carbin. The lottery ticket hypothesis: Finding sparse, trainable neural networks. In *7th International Conference on Learning Representations, ICLR 2019, New Orleans, LA, USA, May 6-9, 2019*. OpenReview.net, 2019. 1, 2
- [14] Shangqian Gao, Feihu Huang, Weidong Cai, and Heng Huang. Network pruning via performance maximization. In *Proceedings of the IEEE/CVF Conference on Computer Vision and Pattern Recognition*, pages 9270–9280, 2021. 1, 2
- [15] Arthur Gretton, Olivier Bousquet, Alex Smola, and Bernhard Schölkopf. Measuring statistical dependence with hilbert-schmidt norms. In *International conference on algorithmic learning theory*, pages 63–77. Springer, 2005. 4
- [16] Song Han, Jeff Pool, John Tran, and William Dally. Learning both weights and connections for efficient neural network. *Advances in neural information processing systems*, 28, 2015. 1, 2
- [17] Song Han, Xingyu Liu, Huizi Mao, Jing Pu, Ardavan Pedram, Mark A Horowitz, and William J Dally. Eie: Efficient inference engine on compressed deep neural network. *ACM SIGARCH Computer Architecture News*, 44(3):243–254, 2016. 2
- [18] David R Hardoon, Sandor Szedmak, and John Shawe-Taylor. Canonical correlation analysis: An overview with application to learning methods. *Neural computation*, 16(12):2639–2664, 2004. 13
- [19] Kaiming He, Xiangyu Zhang, Shaoqing Ren, and Jian Sun. Deep residual learning for image recognition. In *Proceedings of the IEEE conference on computer vision and pattern recognition*, pages 770–778, 2016. 1, 2, 6, 14
- [20] Xia Hu, Lingyang Chu, Jian Pei, Weiqing Liu, and Jiang Bian. Model complexity of deep learning: A survey. *Knowledge and Information Systems*, 63(10):2585–2619, 2021. 2
- [21] Zehao Huang and Naiyan Wang. Data-driven sparse structure selection for deep neural networks. In *Proceedings of the European conference on computer vision (ECCV)*, pages 304–320, 2018. 1, 2
- [22] Barry L Kalman and Stan C Kwasny. Why tanh: choosing a sigmoidal function. In *[Proceedings 1992] IJCNN International Joint Conference on Neural Networks*, pages 578–581. IEEE, 1992. 4
- [23] Simon Kornblith, Mohammad Norouzi, Honglak Lee, and Geoffrey Hinton. Similarity of neural network represen-

- tations revisited. In *International Conference on Machine Learning*, pages 3519–3529. PMLR, 2019. 3, 4, 13
- [24] Alex Krizhevsky, Geoffrey Hinton, et al. Learning multiple layers of features from tiny images. 2009. 6, 14
- [25] Hanwen Liang, Shifeng Zhang, Jiacheng Sun, Xingqiu He, Weiran Huang, Kechen Zhuang, and Zhenguo Li. DARTS+: improved differentiable architecture search with early stopping. *CoRR*, abs/1909.06035, 2019. 1, 14
- [26] Mingbao Lin, Rongrong Ji, Yan Wang, Yichen Zhang, Baochang Zhang, Yonghong Tian, and Ling Shao. Hrank: Filter pruning using high-rank feature map. In *Proceedings of the IEEE/CVF conference on computer vision and pattern recognition*, pages 1529–1538, 2020. 1, 2
- [27] Hanxiao Liu, Karen Simonyan, and Yiming Yang. DARTS: differentiable architecture search. In *7th International Conference on Learning Representations, ICLR 2019, New Orleans, LA, USA, May 6-9, 2019*. OpenReview.net, 2019. 1, 6, 14
- [28] Yuqiao Liu, Yanan Sun, Bing Xue, Mengjie Zhang, and Gary G. Yen. A survey on evolutionary neural architecture search. *CoRR*, abs/2008.10937, 2020. 1, 14
- [29] Zhenhua Liu, Jizheng Xu, Xiulian Peng, and Ruiqin Xiong. Frequency-domain dynamic pruning for convolutional neural networks. *Advances in neural information processing systems*, 31, 2018. 1, 2
- [30] Yao Lu, Wen Yang, Yunzhe Zhang, Zuohui Chen, Jinyin Chen, Qi Xuan, Zhen Wang, and Xiaoni Yang. Understanding the dynamics of dnns using graph modularity. In *Computer Vision—ECCV 2022: 17th European Conference, Tel Aviv, Israel, October 23–27, 2022, Proceedings, Part XII*, pages 225–242. Springer, 2022. 1, 2, 8, 15
- [31] Yao Lu, Yutao Zhu, Yuqi Li, Dongwei Xu, Yun Lin, Qi Xuan, and Xiaoni Yang. A generic layer pruning method for signal modulation recognition deep learning models. *arXiv preprint arXiv:2406.07929*, 2024. 1
- [32] Ana I Maqueda, Antonio Loquercio, Guillermo Gallego, Narciso García, and Davide Scaramuzza. Event-based vision meets deep learning on steering prediction for self-driving cars. In *Proceedings of the IEEE Conference on Computer Vision and Pattern Recognition*, pages 5419–5427, 2018. 1
- [33] Ari Morcos, Maithra Raghu, and Samy Bengio. Insights on representational similarity in neural networks with canonical correlation. *Advances in Neural Information Processing Systems*, 31, 2018. 13
- [34] Thao Nguyen, Maithra Raghu, and Simon Kornblith. Do wide and deep networks learn the same things? uncovering how neural network representations vary with width and depth. In *9th International Conference on Learning Representations, ICLR 2021, Virtual Event, Austria, May 3-7, 2021*. OpenReview.net, 2021. 13
- [35] Adam Paszke, Sam Gross, Francisco Massa, Adam Lerer, James Bradbury, Gregory Chanan, Trevor Killeen, Zeming Lin, Natalia Gimelshein, Luca Antiga, Alban Desmaison, Andreas Köpf, Edward Z. Yang, Zachary DeVito, Martin Raison, Alykhan Tejani, Sasank Chilamkurthy, Benoit Steiner, Lu Fang, Junjie Bai, and Soumith Chintala. Pytorch: An imperative style, high-performance deep learning library. In *Advances in Neural Information Processing Systems 32: Annual Conference on Neural Information Processing Systems 2019, NeurIPS 2019, December 8-14, 2019, Vancouver, BC, Canada*, pages 8024–8035, 2019. 3
- [36] Hieu Pham, Melody Guan, Barret Zoph, Quoc Le, and Jeff Dean. Efficient neural architecture search via parameters sharing. In *Proceedings of the 35th International Conference on Machine Learning*, pages 4095–4104. PMLR, 2018. 1, 14
- [37] Maithra Raghu, Justin Gilmer, Jason Yosinski, and Jascha Sohl-Dickstein. Svcca: Singular vector canonical correlation analysis for deep learning dynamics and interpretability. *Advances in neural information processing systems*, 30, 2017. 13
- [38] Esteban Real, Sherry Moore, Andrew Selle, Saurabh Saxena, Yutaka Leon Suematsu, Jie Tan, Quoc V. Le, and Alexey Kurakin. Large-scale evolution of image classifiers. In *Proceedings of the 34th International Conference on Machine Learning*, pages 2902–2911. PMLR, 2017. 1, 14
- [39] Esteban Real, Alok Aggarwal, Yanping Huang, and Quoc V. Le. Regularized evolution for image classifier architecture search. In *The Thirty-Third AAAI Conference on Artificial Intelligence, AAAI 2019, The Thirty-First Innovative Applications of Artificial Intelligence Conference, IAAI 2019, The Ninth AAAI Symposium on Educational Advances in Artificial Intelligence, EAAI 2019, Honolulu, Hawaii, USA, January 27 - February 1, 2019*, pages 4780–4789. AAAI Press, 2019. 1, 6, 14
- [40] Joseph Redmon, Santosh Divvala, Ross Girshick, and Ali Farhadi. You only look once: Unified, real-time object detection. In *Proceedings of the IEEE conference on computer vision and pattern recognition*, pages 779–788, 2016. 1
- [41] Olga Russakovsky, Jia Deng, Hao Su, Jonathan Krause, Sanjeev Satheesh, Sean Ma, Zhiheng Huang, Andrej Karpathy, Aditya Khosla, Michael S. Bernstein, Alexander C. Berg, and Li Fei-Fei. Imagenet large scale visual recognition challenge. *International Journal of Computer Vision*, 115(3): 211–252, 2015. 6, 14
- [42] Karen Simonyan and Andrew Zisserman. Very deep convolutional networks for large-scale image recognition. In *3rd International Conference on Learning Representations, ICLR 2015, San Diego, CA, USA, May 7-9, 2015, Conference Track Proceedings*, 2015. 6, 13
- [43] Le Song, Alex Smola, Arthur Gretton, Justin Bedo, and Karsten Borgwardt. Feature selection via dependence maximization. *Journal of Machine Learning Research*, 13(5), 2012. 4
- [44] Yang Sui, Miao Yin, Yi Xie, Huy Phan, Saman Aliari Zonouz, and Bo Yuan. Chip: Channel independence-based pruning for compact neural networks. *Advances in Neural Information Processing Systems*, 34, 2021. 1, 2
- [45] Mingxing Tan, Bo Chen, Ruoming Pang, Vijay Vasudevan, Mark Sandler, Andrew Howard, and Quoc V Le. Mnasnet: Platform-aware neural architecture search for mobile. In *Proceedings of the IEEE/CVF Conference on Computer Vision and Pattern Recognition*, pages 2820–2828, 2019. 1, 2, 5, 6

- [46] Hui Tang, Yao Lu, and Qi Xuan. Sr-init: An interpretable layer pruning method. In *ICASSP 2023-2023 IEEE International Conference on Acoustics, Speech and Signal Processing (ICASSP)*, pages 1–5. IEEE, 2023. 1
- [47] Yehui Tang, Yunhe Wang, Yixing Xu, Yiping Deng, Chao Xu, Dacheng Tao, and Chang Xu. Manifold regularized dynamic network pruning. In *Proceedings of the IEEE/CVF Conference on Computer Vision and Pattern Recognition*, pages 5018–5028, 2021. 1, 2
- [48] Wenxiao Wang, Shuai Zhao, Minghao Chen, Jinming Hu, Deng Cai, and Haifeng Liu. Dbp: discrimination based block-level pruning for deep model acceleration. *arXiv preprint arXiv:1912.10178*, 2019. 8, 15
- [49] Wenxiao Wang, Minghao Chen, Shuai Zhao, Long Chen, Jinming Hu, Haifeng Liu, Deng Cai, Xiaofei He, and Wei Liu. Accelerate cnns from three dimensions: A comprehensive pruning framework. In *International Conference on Machine Learning*, pages 10717–10726. PMLR, 2021. 1, 2, 13
- [50] Thomas Wolf, Lysandre Debut, Victor Sanh, Julien Chaumond, Clement Delangue, Anthony Moi, Pierric Cistac, Tim Rault, Rémi Louf, Morgan Funtowicz, Joe Davison, Sam Shleifer, Patrick von Platen, Clara Ma, Yacine Jernite, Julien Plu, Canwen Xu, Teven Le Scao, Sylvain Gugger, Mariama Drame, Quentin Lhoest, and Alexander M. Rush. Transformers: State-of-the-art natural language processing. In *Proceedings of the 2020 Conference on Empirical Methods in Natural Language Processing: System Demonstrations, EMNLP 2020 - Demos, Online, November 16-20, 2020*, pages 38–45. Association for Computational Linguistics, 2020. 3
- [51] Bichen Wu, Xiaoliang Dai, Peizhao Zhang, Yanghan Wang, Fei Sun, Yiming Wu, Yuandong Tian, Peter Vajda, Yangqing Jia, and Kurt Keutzer. Fbnet: Hardware-aware efficient convnet design via differentiable neural architecture search. In *Proceedings of the IEEE/CVF Conference on Computer Vision and Pattern Recognition*, pages 10734–10742, 2019. 2, 5
- [52] Lingxi Xie and Alan L. Yuille. Genetic CNN. In *IEEE International Conference on Computer Vision, ICCV 2017, Venice, Italy, October 22-29, 2017*, pages 1388–1397. IEEE Computer Society, 2017. 1, 14
- [53] Sirui Xie, Hehui Zheng, Chunxiao Liu, and Liang Lin. SNAS: stochastic neural architecture search. In *7th International Conference on Learning Representations, ICLR 2019, New Orleans, LA, USA, May 6-9, 2019*. OpenReview.net, 2019. 5
- [54] Tianyun Zhang, Shaokai Ye, Kaiqi Zhang, Jian Tang, Wujie Wen, Makan Fardad, and Yanzhi Wang. A systematic dnn weight pruning framework using alternating direction method of multipliers. In *Proceedings of the European Conference on Computer Vision (ECCV)*, pages 184–199, 2018. 1, 2
- [55] Zhao Zhong, Junjie Yan, Wei Wu, Jing Shao, and Cheng-Lin Liu. Practical block-wise neural network architecture generation. In *Proceedings of the IEEE Conference on Computer Vision and Pattern Recognition (CVPR)*, 2018. 1, 14
- [56] Yao Zhou, Gary G Yen, and Zhang Yi. Evolutionary shallow-ing deep neural networks at block levels. *IEEE Transactions on Neural Networks and Learning Systems*, 2021. 13
- [57] Barret Zoph and Quoc V. Le. Neural architecture search with reinforcement learning. In *5th International Conference on Learning Representations, ICLR 2017, Toulon, France, April 24-26, 2017, Conference Track Proceedings*. OpenReview.net, 2017. 6, 14
- [58] Barret Zoph, Vijay Vasudevan, Jonathon Shlens, and Quoc V. Le. Learning transferable architectures for scalable image recognition. In *Proceedings of the IEEE Conference on Computer Vision and Pattern Recognition (CVPR)*, 2018. 1, 14

A. Additional Experiments on Redundancy-aware NAS

In this section, we incorporate Params and FLOPs instead of Latency into the scoring function and depict the scoring function as follows:

$$\begin{aligned} \max_m \quad ACC(m) \times \left[\lambda \times \frac{Para(m)}{P} + (1 - \lambda) \times \frac{MSRS(m)}{M} \right]^w, \\ \max_m \quad ACC(m) \times \left[\lambda \times \frac{FLOP(m)}{F} + (1 - \lambda) \times \frac{MSRS(m)}{M} \right]^w, \end{aligned}$$

where $Para(m)$, P , $FLOP(m)$ and F denote Params of model m , expected Params, FLOPs of model m and expected FLOPs, respectively. Meanwhile, the scoring functions of S2 are formalized as follows:

$$\begin{aligned} \max_m \quad ACC(m) \times \left[\frac{Para(m)}{P} \right]^w, \\ \max_m \quad ACC(m) \times \left[\frac{FLOP(m)}{F} \right]^w, \end{aligned}$$

Specifically, we respectively sample 11715, 11748 and 11741 valid architecture candidates on CIFAR10, CIFAR100 and ImageNet16-120 in the topology search space of NATS-Bench and utilize Algorithm 2 to select top-ranking models. As for redundancy-aware NAS using FLOPs, we select 1‰ top-ranking models. As for redundancy-aware NAS using Params, we select 5‰ top-ranking models on CIFAR10 and CIFAR100, 0.5‰ top-ranking models on ImageNet16-120. Tab. E3 and Tab. E4 provide the detailed experimental parameter settings. As shown in Fig. E5, we can draw the same conclusion that our redundancy-aware NAS is proficient at selecting models with less redundancy and better performance.

B. How to pick expected MSRS

In this section, we elaborate on the empirical guide to picking expected MSRS as a budget. Before that, we first explore the similarity matrices of ResNets on CIFAR10 (see Fig. E7). We observe that values with high similarity tend to take on a triangular shape as layers deepens. We believe that is because many successive layers are essentially repeating the same operation multiple times, refining features just a little more each time. Hence, these successive layers are highly similar, resulting in the triangular shape for high similarity values in similarity matrices. On the basis of this finding, we assume that the redundancy is quadratic with number of layers (depth) of the given model. In order to further verify our conjecture, we fit a quadratic function of depth with respect to MSRS according to the commonly used ResNets, which is shown in Fig. E4. We find that the fitted curve is almost coincides with the original curve, which confirms our conjecture. Afterwards, we revisit the similarity matrix of shallow models. We find that values

with high similarity are rare and show a scatter-like distribution (see the left plot of Fig. E7). Hence, we boldly guess that MSRS should be proportional to the layer depth. Next we empirically pick up multiple low-redundancy models with different depths and fit linear functions on CIFAR10 and CIFAR100, which are formalized as follows:

$$\begin{aligned} M_{C10} &= \begin{cases} 0 & l \leq 14 \\ 7.6 \times l - 106.4 & l > 14 \end{cases}, \\ M_{C100} &= \begin{cases} 0 & l \leq 3 \\ 2.4 \times l - 8.27 & l > 3 \end{cases}, \end{aligned}$$

where l denotes the model depth. C10 and C100 are CIFAR10 and CIFAR100.

C. Experimental setup

C.1. Dataset Description

CIFAR10 and CIFAR100 consist of 50K training images and 10K testing images in 10 and 100 fine-grained classes, respectively. ImageNet spans 1,000 classes and contains 1.28M training images and 50K validation images. ImageNet16-120 consists of 151.7K training images, 3K validation images, and 3K testing images, whose images are down-sampled from the original ImageNet to 16×16 pixels and selected from ImageNet with label $\in [1, 120]$. Appendix E in Appendix provides a brief description of the datasets statistics.

C.2. Hyperparameter Settings

If not specified, we utilize minibatch of size $n = 256$ and $\beta = 100$ to calculate MSRS. As for model-specific threshold ϵ , we set $\epsilon = 0.7$ for models of plain structure (e.g., VGGs) and $\epsilon = 0.8$ for models of block structure (e.g., ResNets). More discussions on the selection of these configurations are presented in Appendix C.3. Besides, for calculating MSRS, we repeat each configuration 10 times and report the averaged results to counteract the effects potentially brought by randomness.

C.3. Hyperparameter Selection of MSRS

Batch size n , scaling factor β and model-specific threshold ϵ are three configurable parameters in calculating MSRS. If not specified, we utilize minibatch of size $n = 256$ and $\beta = 100$ to calculate MSRS. As for model-specific threshold ϵ , we set $\epsilon = 0.7$ for models of plain structure (e.g., VGGs) and $\epsilon = 0.8$ for models of block structure (e.g., ResNets). In this section, we aim to discuss the effect of them on MSRS.

Since $HSIC_0$ is a biased estimator with $O(\frac{1}{n})$ bias. In order to reduce the impacts of batch size on the value of MSRS, we utilize an unbiased estimator of $HSIC_1$ in place of $HSIC_0$. It can be reasonable to question whether

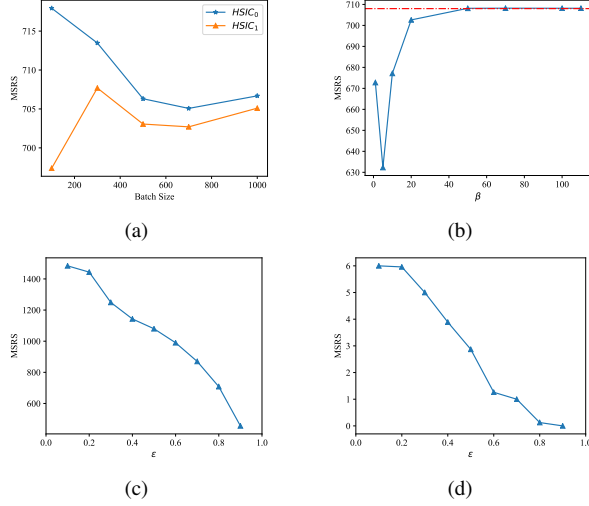


Figure C1. Results for different settings of HSIC, β and ϵ .

$HSIC_1$ is independent of the batch size. Therefore, we conduct experiments with ResNet110 on CIFAR10 with configurations of $n = 100, 300, 500, 700, 1,000$ and $\beta = 100$. Fig. C1a presents the relationship between batch size and MSRS calculated by $HSIC_0/HSIC_1$. In contrast to MSRS calculated by $HSIC_0$, MSRS calculated by $HSIC_1$ is less sensitive to changes in n (the standard deviation is 3.4 for MSRS calculated by $HSIC_1$ while 5.0 for MSRS calculated by $HSIC_0$). Since batch size has a negligible effect on MSRS calculated by $HSIC_1$, in this paper we uniformly take $n = 256$.

As for scaling factor β , we utilize $\beta = 1, 5, 10, 20, 50, 70, 100, 110$ (If $\beta > 110$, the result will be out of range for floating point representation in Python⁴, so we take β as maximum as 110) and $n = 256$ to conduct experiments with ResNet110 on CIFAR10. As shown in Fig. C1b, when $\beta \geq 50$, MSRS tends to be stable. So, empirically it is indeed possible to fix β to a certain value ≥ 50 . In this work, we utilize $\beta = 50$ for the sake of uniformity.

As for model-specific threshold ϵ , we conducted experiments with ResNet110 on CIFAR10, using $\beta = 100$, changing ϵ from 0.1 to 0.9. As shown in Fig. C1c, MSRS is indeed sensitive (inversely proportional) to ϵ . Hence, the selection of ϵ is critical for calculating MSRS. Next, we introduce a heuristic method to choose ϵ . Due to the space limitation, we only introduce the selection of ϵ for models of block structure here. First, we choose a well-trained ResNet8 on CIFAR10 with 85.41% test accuracy. Obviously, ResNet8 is underfitting on CIFAR10 and we believe it has no model structural redundancy. Afterwards, we use different ϵ with $\beta = 100$, $n = 256$ to calculate MSRS, which is shown in Fig. C1d. We observe that when $\epsilon = 0.8$,

MSRS is close to 0, and thus utilize it for models of block structure.

D. Related Work

Representational Similarity Metrics: Representational similarity computes the similarity between statistics on two different IRs, which gives insight into the interaction between machine learning algorithms and data than the value of the loss function alone. There exist several statistical measures, each of which serves as a different notion of similarity. Haroon et al. [18] propose canonical correlation analysis (CCA), which aims to find basis vectors such that the correlation between the projections of variables onto these basis vectors is mutually maximized. Since CCA is sensitive to perturbation, Raghu et al. [37] and Morcos et al. [33] propose Singular Vector CCA and Projection Weighted CCA to reduce the sensitivity of CCA to perturbation, respectively. However, these metrics are invariant to invertible linear transformation and can not measure meaningful similarities between IRs of higher dimensions than the number of data points. To address the above challenges, Kornblith et al. [23] introduce CKA to measure similarities between IRs. Nguyen et al. [34] investigate the effects of depth and width on IRs on the basis of CKA, and find that overly complicated models exhibit the block structure. Different from these works, which purely compute the representational similarity, we associate representational similarity with model structural redundancy. Furthermore, we explore the redundancy issues in state-of-the-art DNNs.

Layer Pruning: The core of layer pruning lies in the selection of layers, which should achieve the lowest compromise in accuracy with the highest compression ratio. Chen et al. [3] fit a linear classifier to evaluate the performance of a layer thus finding the ones to be removed. On the basis of [3], Elkerdawy et al. [12] utilize imprinting to efficiently approximate the accuracy of each layer and prune the layer which achieves minimal accuracy improvement compared to the preceding layer. Zhou et al. [56] reconstruct the loss of layer pruning as a dual-objective function that minimizes the error and number of blocks, and further adopts multi-objective evolutionary algorithm to solve it. Wang et al. [49] formalize the relationships between accuracy and depth/width/resolution as a polynomial regression and obtain the optimal values for these dimensions by solving the polynomial regression. De et al. [7] replace the last few layers with an auxiliary network as an effective interpreter of IRs to produce the pruned model. Unlike the existing works, we propose a redundancy-aware layer pruning method with the guidance of layer similarity to remove those redundant layers, which has been demonstrated to be superior to existing works by extensive experimental results.

NAS: Since the state of the arts, e.g., VGG [42] and

⁴<https://www.python.org>

ResNet [19] are manually designed by experts by a trial-and-error process, which requires substantial resources and time even for experts. To cope with the aforementioned challenges, NAS, as a technique for automating the architecture designs of DNNs is proposed to reduce onerous development costs. For example, [28, 38, 39, 52] leverage evolutionary algorithms to search for novel architectures automatically. Besides, Zoph et al. [57] utilize a recurrent neural network (RNN) as a controller to compose neural network architectures and train this RNN with reinforcement learning to obtain optimal architectures on a validation set. Then many follow-up methods [2, 36, 55, 58] improve this framework with different controller policies and neural architecture encoding. Compared to the above-mentioned studies sampling architectures from a discrete search space, some works [4, 25, 27] search over a continuous and differentiable search space, which can be optimized with gradient descent. Generally speaking, NAS aims to search for the optimal architecture for a given resource budget that achieves an accuracy-budget trade-off. Unfortunately, as we mentioned in our paper, existing resource budgets (e.g., Latency) can not quantitatively measure the remaining redundancy in DNN models. To bridge this gap, we propose MSRS to quantitatively assess the degree of redundancy in the model structure, and further present a redundancy-aware NAS algorithm to search for the optimal architecture.

E. Discussion and Threats to Validity

This subsection summarizes the findings and insights obtained in this paper and followed by the threats to validity of our work.

Discussion. This paper proposes a testing metric called MSRS to quantitatively measure the degree of redundancy in DNN models. With MSRS, we systematically investigate the redundancy issue in DNN models and confirm the ubiquitous presence of model redundancy, sometimes even to a surprisingly high level, which urgently calls for model structure optimization. Equipped with MSRS, we further present a novel testing framework REDTEST, with the aim to facilitate further studies on optimizing model structures in a more computationally effective environment. Our large-scale study marks the first step towards such a direction, with interesting findings identified.

Threats to validity. The selection of subject datasets and models could be a threat to validity. We try to counter this by using four publically available datasets with diverse scales, together with a large collection of widely used DNN models that achieve competitive performance. A further threat would be the randomness factors for computing MSRS. We try to counteract the effects potentially brought by randomness by repeating each configuration 10 times and reporting the averaged results.

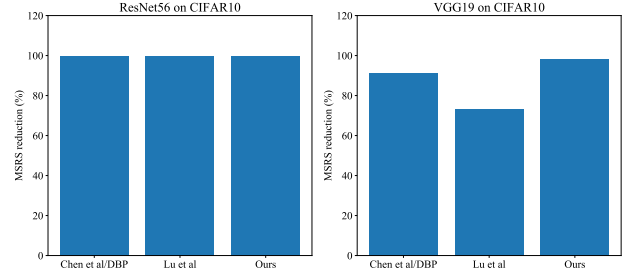


Figure E2. MSRS reduction after layer pruning.

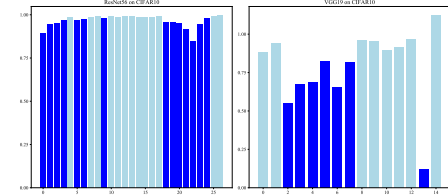


Figure E3. CKA values of two adjacent layers. The bars with the transparent color represent that the current layers are similar to their front layer and are considered redundant.

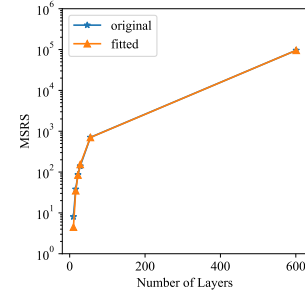


Figure E4. The relationship between the number of layers and MSRS.

Datasets	Image Size	Training	Testing	Classes
CIFAR10 [24]	32, 32, 3	50K	10K	10
CIFAR100 [24]	32, 32, 3	50K	10K	100
ImageNet [41]	224, 224, 3	1.28M	50K	1000
ImageNet16-120 [6]	16, 16, 3	151.7K	3K	120

Table E1. Datasets characteristics.

Dataset	Number of models	T	M	w	λ
CIFAR10	11715	0.01	35	-0.20	0.1
CIFAR100	11748	0.01	35	-0.24	0.2
ImageNet16-120	11741	0.01	35	-0.20	0.5

Table E2. Hyperparameter settings of redundancy-aware NAS using Latency.

Dataset	Number of models	P	M	w	λ
CIFAR10	11715	0.15	35	-0.035	0.4
CIFAR100	11748	0.15	35	-0.06	0.8
ImageNet16-120	11741	0.15	35	-0.073	0.2

Table E3. Hyperparameter settings of redundancy-aware NAS using Params.

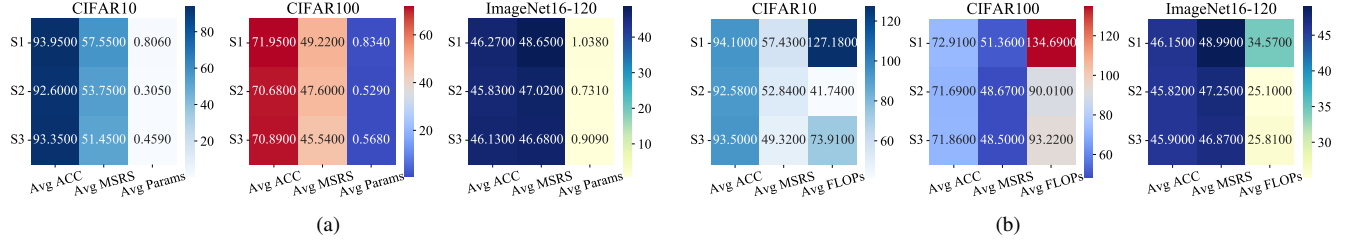


Figure E5. Statistics of top-ranking models. Avg ACC (%), Avg MSRS, Avg Params (M), and Avg FLOPs (M) represent average accuracy, average MSRS, average Params, and average FLOPs, respectively.

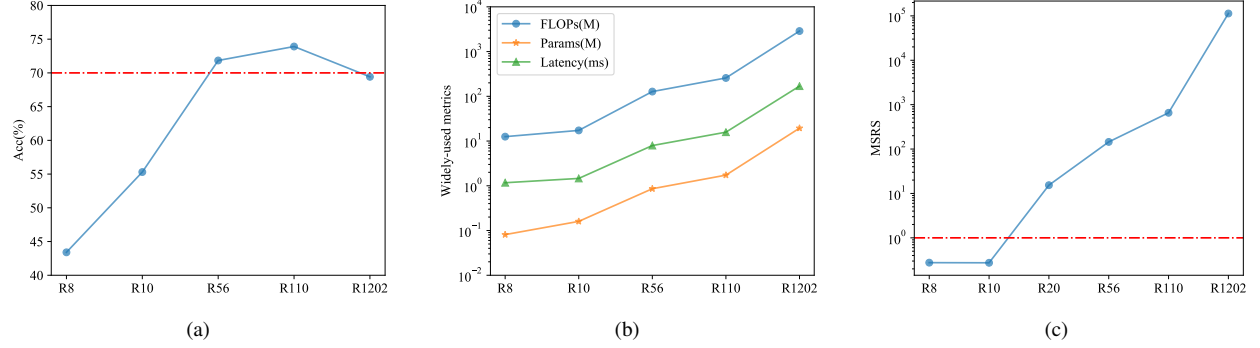


Figure E6. Differences between existing metrics and MSRS for a family of ResNets on CIFAR100. R denotes ResNet.

Dataset	Number of models	F	M	w	λ
CIFAR10	11715	10	35	-0.03	0.15
CIFAR100	11748	10	35	-0.06	0.4
ImageNet16-120	11741	10	35	-0.073	0.6

Table E4. Hyperparameter settings of redundancy-aware NAS using FLOPs.

Model	Method	Top-1%	Params(PR)	FLOPs(PR)	Latency(PR)
ResNet56	Original	71.81	0%	0%	0%
	Chen et al. [3]/DBP [48]	70.45 ± 0.18	36.67%	41.39%	39.53%
	Lu et al. [30]	69.24 ± 0.10	10.83%	41.65%	37.94%
	Ours	70.09 ± 0.10	31.32%	48.99%	45.78%
VGG19	Original	72.63	0%	0%	0%
	Chen et al. [3]/DBP [48]	69.73 ± 0.15	71.81%	45.00%	40.70%
	Lu et al. [30]	66.88 ± 0.25	41.19%	45.00%	40.35%
	Ours	70.33 ± 0.44	54.63%	52.00%	38.60%

Table E5. Experimental results on the CIFAR100 dataset using VGG19 and ResNet56, PR is the pruning rate.

	VGGs				ResNets ¹				
	VGG11	VGG13	VGG16	VGG19	ResNet20(18)	ResNet32(34)	ResNet44(50)	ResNet56(101)	ResNet110(152)
CIFAR10	92.11%	93.68%	93.63%	93.36%	91.78%	92.38%	92.92%	93.11%	93.78%
CIFAR100	66.87%	70.19%	72.34%	72.63%	58.61%	69.78%	71.32%	71.81%	73.91%
ImageNet	70.36%	71.55%	73.48%	74.17%	69.67%	73.22%	75.99%	77.32%	78.26%

¹ We train ResNet20, 32, 44, 56, 110 on CIFAR10 and CIFAR100, ResNet18, 34, 50, 101, 152 on ImageNet.

Table E6. Models Performance.

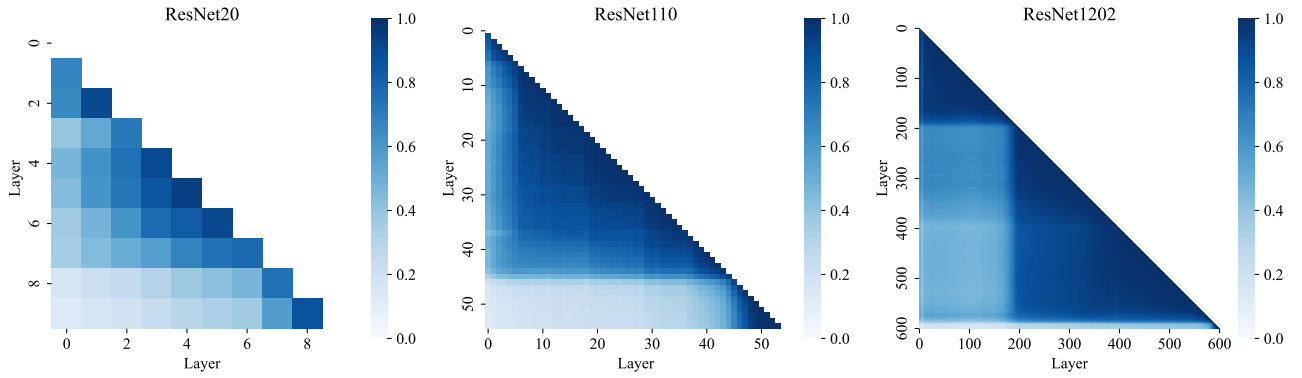


Figure E7. The lower triangular similarity matrices of ResNets on CIFAR10. The darker the color, the more similar.